Dynamics of Continuous, Discrete and Impulsive Systems
Series **B:** *Applications & Algorithms* **25 (2018)** 219-231

A SHALLOW WATER MODEL OF THE SOLAR TACHOCLINE: A NUMERICAL APPROACH TO DETERMINE WAVE STRUCTURE

F.J. Poulin[1], A. Borissov[2], B.A. Storer[1],and M. Stastna[1]

[1]Department of Applied Mathematics
University of Waterloo, Waterloo, Ontario N2L 3G1, Canada
[2]School of Mathematics and Statistics
University of St Andrews, St Andrews, Fife KY16 9SS, Scotland

Abstract. We revisit the Magneto-Hydrodynamic Shallow Water model of the solar tachocline originally presented in [3]. First, we demonstrate that the spherical linearized equations considered in [13] have an extra restriction that is not required and that the error in their model increases with the increasing strength of the magnetic field and the ambient rotation of the star. Second, we present a simple pseudo-spectral model that is able to accurately solve for the modal structure of these solar waves in either the Cartesian or spherical co-ordinate geometries. We demonstrate that even though the asymptotic solution can be fairly good in the presence of strong magnetic fields and strong rotation, the numerical method that we present yields a higher level of accuracy with little computational effort.

Keywords. Solar tachocline, Shallow water model, Magnetohydrodynamics, Wave Dynamics and Pseudospectral approximation

1 Introduction

Helioseismological observations suggest that the Sun possesses a thin fluid layer between the radiative zone, which exhibits solid body rotation, and the outer convective zone, which is differentially rotating [6, 11]. This layer is now referred to as the solar tachocline. It was first suggested by [3] that a Magneto-Hydrodynamic Rotating Shallow Water (MSW) model could be used to model these thin layers. Shallow water models have previously been used mostly for atmospheric and oceanic flows [7].

The three different wave types that can occur in this idealized model of the tachocline are magneto-Poincaré, Rossby and Alfvén waves. This is in contrast to the classical shallow water model in which only Poincaré and Rossby waves are possible (additional wave types are possible in the presence of bottom bathymetry or side walls). The propagation of waves in the solar

tachocline is thought to be of importance to many phenomena involving magnetic activity, including the solar cycle [9], and its long term variability [14]. Furthermore, wave propagation is an important means through which momentum is transported.

Analyses of the linearized equations have been carried out in the context of an f-plane [10], a β-plane, and also in spherical coordinates for varying background magnetic fields: first in [13], hence referred to as ZOBS, and subsequently in [4]. Numerical approaches to the MSW equations have also been implemented in [1] to study the time evolution of the nonlinear dynamics. We complement previous works by presenting a relatively simple numerical model that can be used to determine the spectrum and spatial structures of all the different wave types in this model. We also point out that the analytical solution of ZOBS is more restrictive than perhaps was previously stated in that it assumes the motion is incompressible in two-spatial dimensions.

The outline of this paper is as follows. In section 2 we present the Cartesian and spherical models and show how they can be solved numerically to determine the characteristics of the linear waves in the MSW model. Next, in section 3 we show some numerical results and compare the numerical results with the analytical solution of ZOBS. Finally, we provide conclusions and some directions for future work.

2 Idealized Models and Numerical Methods

The governing equations for fully nonlinear motion of the MSW model that determine the evolution of the linear momentum, mass and magnetic field, as presented in [3] and ZOBS for example, read:

$$\frac{\partial \mathbf{B}}{\partial t} + (\mathbf{u}\cdot\nabla)\,\mathbf{B} = (\mathbf{B}\cdot\nabla)\,\mathbf{u}, \tag{1}$$

$$\frac{\partial \mathbf{u}}{\partial t} + (\mathbf{u}\cdot\nabla)\,\mathbf{u} = \frac{1}{4\pi\mu_0\rho}(\mathbf{B}\cdot\nabla)\,\mathbf{B} - g\nabla H, \tag{2}$$

$$\frac{\partial H}{\partial t} + \nabla\cdot(H\mathbf{V}) = 0. \tag{3}$$

Note that $\mathbf{u}, \mathbf{B}$ and H are the velocity, magnetic field and height, respectively. Physically, these determine how the dynamics must evolve in order to conserve magnetism, momentum and mass, respectively.

As the name implies, a necessary assumption for this shallow water hydrodynamic model to be applicable is that the aspect ratio between the vertical and horizontal scales of motion is small. The tachocline of the Sun has a thickness that is 4% of the solar radius and is located at 0.7 solar radii from the centre where the radius is $6.96 \times 10^8\, m$ [2]. Therefore, this model may be insightful in characterizing some aspects of solar dynamics, in particular some solar waves. With this goal in mind we restrict our attention to the linearized equations about a state of rest and a zonal magnetic field. This

allows us to characterize the different types of waves that can occur and the mechanisms through which they propagate. This limit will always be valid in the regime of very small deviations from the basic state. In the following two subsections we present the model equations for the Cartesian and Spherical MSW models and how they can be treated numerically.

2.1 Cartesian MSW Model

If we are studying flows that have relatively small variations in latitude, then one can make what is often referred to as the β-plane approximation [7]. Linearizing this set of equations in Cartesian co-ordinates yields the following equations for fluid motion on a plane:

$$\frac{\partial u_x}{\partial t} - f u_y = \frac{B_0}{4\pi\mu_0\rho}\frac{\partial b_x}{\partial x} - g\frac{\partial h}{\partial x}, \tag{4}$$

$$\frac{\partial u_y}{\partial t} + f u_x = \frac{B_0}{4\pi\mu_0\rho}\frac{\partial b_y}{\partial x} - g\frac{\partial h}{\partial y}, \tag{5}$$

$$\frac{\partial b_x}{\partial t} = B_0\frac{\partial u_x}{\partial x}, \tag{6}$$

$$\frac{\partial b_y}{\partial t} = B_0\frac{\partial u_y}{\partial x}, \tag{7}$$

$$\frac{\partial h}{\partial t} + H_0\left(\frac{\partial u_x}{\partial x} + \frac{\partial u_y}{\partial y}\right) = 0. \tag{8}$$

Note that u_x, u_y are the two components of velocity, b_x, b_y are the two components of magnetism and h are height. Subscripts denote a particular horizontal direction. We have taken the background magnetic field to be $\mathbf{B} = B_0\hat{x}$, with B_0 constant, and make the beta-plane approximation to the Coriolis parameter $f = 2\Omega\sin\theta \approx f_0 + \beta y$ with $f_0 = 2\Omega\sin\theta_0$ and $\beta = 2\frac{\Omega}{R_0}\cos\theta_0$, where R_0 and Ω are the radius of the star and rotation rates, respecitvely.

To obtain wave solutions we look for normal mode solutions with respect to the zonal direction and time of the form

$$\mathbf{V} = \begin{bmatrix} u_x \\ u_y \\ b_x \\ b_y \\ h \end{bmatrix} = e^{i(k_x x - \omega t)} \begin{bmatrix} \tilde{u}_x \\ \tilde{u}_y \\ \tilde{b}_x \\ \tilde{b}_y \\ \tilde{h} \end{bmatrix}. \tag{9}$$

To study waves that are constrained to propagate zonally within certain specified latitudes, it is convenient to impose no-normal flow boundary conditions at the latitudinal boundaries of the domain: $u_y = 0$ at $y = \pm\frac{L}{2}$ where L is the width of the channel. Even though there are no such boundaries in stars, this choice is convenient for the numerical calculations and is appropriate in describing waves that propagate in the East-West directions [8].

Substituting this into equations (4)-(8) we get the system $\mathbf{MV} = i\omega\mathbf{V}$ where

$$\mathbf{M} = \begin{bmatrix} 0 & -f & -\frac{B_0 ik_x}{\mu_0 \rho} & 0 & gik_x \\ f & 0 & 0 & -\frac{B_0 ik_x}{\mu_0 \rho} & g\frac{\partial}{\partial y} \\ -B_0 ik_x & 0 & 0 & 0 & 0 \\ 0 & -B_0 ik_x & 0 & 0 & 0 \\ H_0 ik_x & H_0 \frac{\partial}{\partial y} & 0 & 0 & 0 \end{bmatrix}. \tag{10}$$

Note that this system is mathematically equivalent to equation (14) of ZOBS; however, instead of writing the eigenvalue problem as a second order scalar equation we prefer to write it as a first order system of five equations, which we can then solve numerically. To achieve high numerical accuracy for a given number of degrees of freedom, we will use a spectral method on a Chebyshev grid [12], which we will discuss in detail later in this section.

2.2 Spherical MSW Model

A more general approach to study the MSW equations (1)-(3) is instead to assume a spherical geometry where ϕ is longitude and θ is co-latitude. In this case we assume the background magnetic field in the ϕ-direction given by $B_\phi = B_0 \sin\theta$ and the governing linearized equations are,

$$\frac{\partial u_\theta}{\partial t} - 2\Omega_0 \cos\theta u_\phi = \frac{B_0}{4\pi\mu_0\rho R_0}\frac{\partial b_\theta}{\partial \phi} - 2\frac{B_0}{4\pi\mu_0\rho R_0}\cos\theta b_\phi - \frac{g}{R_0}\frac{\partial h}{\partial \theta}, \tag{11}$$

$$\frac{\partial u_\phi}{\partial t} + 2\Omega_0 \cos\theta u_\theta = \frac{B_0}{4\pi\mu_0\rho R_0}\frac{\partial b_\phi}{\partial \phi} + 2\frac{B_0}{4\pi\mu_0\rho R_0}\cos\theta b_\theta - \frac{g}{R_0 \sin\theta}\frac{\partial h}{\partial \phi} \tag{12}$$

$$\frac{\partial b_\theta}{\partial t} = \frac{B_0}{R_0}\frac{\partial u_\theta}{\partial \phi}, \tag{13}$$

$$\frac{\partial b_\phi}{\partial t} = \frac{B_0}{R_0}\frac{\partial u_\phi}{\partial \phi}, \tag{14}$$

$$\frac{\partial h}{\partial t} = -\frac{H_0}{R_0}\frac{\partial u_\theta}{\partial \theta} - \frac{H_0 \cos\theta}{R_0 \sin\theta}u_\theta - \frac{H_0}{R_0 \sin\theta}\frac{\partial u_\phi}{\partial \phi}. \tag{15}$$

This system can similarly be written as $\mathbf{MV} = i\omega\mathbf{V}$ but with solution vector $\mathbf{V}$ and dynamic matrix $\mathbf{M}$ can be written as,

$$\mathbf{V} = \begin{bmatrix} u_\theta \\ u_\phi \\ b_\theta \\ b_\phi \\ h \end{bmatrix} = e^{i(s\phi - \omega t)} \begin{bmatrix} \tilde{u}_\theta \\ \tilde{u}_\phi \\ \tilde{b}_\theta \\ \tilde{b}_\phi \\ \tilde{h} \end{bmatrix},$$

and the matrix is

$$\begin{bmatrix} 0 & -2\Omega_0\cos\theta & -\frac{isB_0}{4\pi\mu_0\rho R_0} & \frac{2B_0}{4\pi\mu_0\rho R_0}\cos\theta & \frac{g}{R_0}\frac{\partial}{\partial\theta} \\ 2\Omega_0\cos\theta & 0 & -\frac{2B_0}{4\pi\mu_0\rho R_0}\cos\theta & -\frac{isB_0}{4\pi\mu_0\rho R_0} & \frac{isg}{R_0\sin\theta} \\ -\frac{isB_0}{R_0} & 0 & 0 & 0 & 0 \\ 0 & -\frac{isB_0}{R_0} & 0 & 0 & 0 \\ \frac{H_0}{R_0}\left(\frac{\cos\theta}{\sin\theta}+\frac{\partial}{\partial\theta}\right) & \frac{isH_0}{R_0\sin\theta} & 0 & 0 & 0 \end{bmatrix}$$

This system of equations is nearly equivalent to that presented in ZOBS. In the Appendix we go through the details of why our equation (14) differs from equation (26) in ZOBS. An alternative way to see the limitation of their equation is to make the assumption that the variations in latitude are small and then recover the β-plane equations. As is well explained in [7], in this limit of a β-plane we have that $[u_\theta, u_\phi, b_\theta, b_\phi] \to [u_x, u_y, b_x, b_y]$ and furthermore,

$$\frac{1}{R_0\sin\theta}\frac{\partial}{\partial\phi} \approx \frac{\partial}{\partial x} \qquad \text{and} \qquad \frac{1}{R_0}\frac{\partial}{\partial\theta} \approx \frac{\partial}{\partial y}. \tag{16}$$

The ZOBS version of the meridional magnetic equation yields that $\partial u_x/\partial x$ is instead replaced by $-\partial u_y/\partial y$. This is only strictly true in the two-dimensional incompressible limit, what is referred to in the oceanographic community as the rigid-lid approximation. This is probably a reasonable approximation in many instances, however, our use of a spectral collocation numerical method allows us to achieve a more accurate solution of the general model than can be obtained by any asymptotic solution. This allows us to show that the analytical solution of ZOBS is appropriate for a wide range of parameters and it also illustrates the structure of these waves in the limit where the ZOBS solution is no longer valid.

2.3 Numerical Method

By finding numerical approximations to the eigenvalues and eigenvectors of the eigensystem above we determine the frequencies and spatial structure of the solar-SW waves that are admissible in this system. This is done by discretizing the meridional direction onto a Chebyshev grid and using the corresponding differentiation matrix as presented in [12]. Details of how this has been successfully applied in the oceanographic context can be found in [8] and many subsequent works. In our numerical results for both the Cartesian and the Spherical models we found that using only 100 grid points yielded accurate solutions. This calculation was performed very efficiently using the the direct solver `eig` in Octave/Matlab based on LAPACK.

3 Spatial Structure of Wave Solutions

We have used the numerical method explained in the previous section to compute the spatial structure and frequencies for a variety of modes that idealize

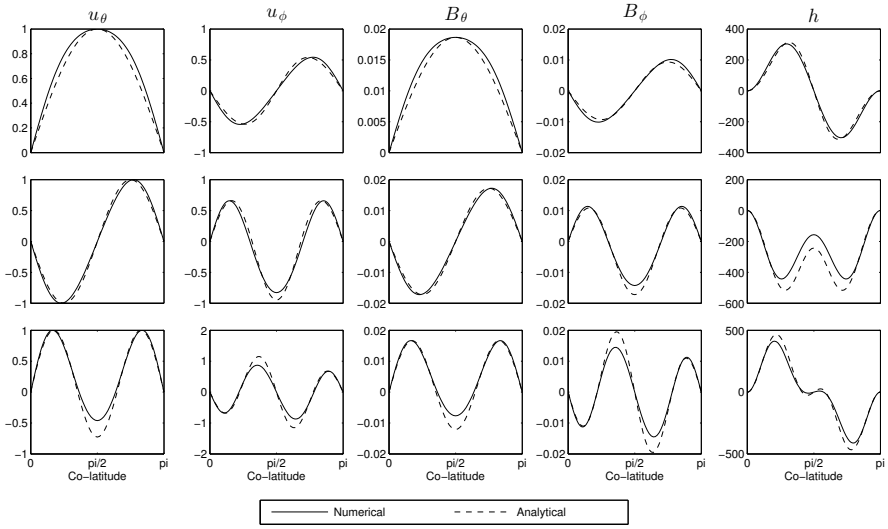

Figure 1: Comparison of the MSW modes computed numerically to the asymptotic solution presented in ZOBS [13]. Columns one to five depict the following fields: $u_\theta, u_\phi, B_\theta, B_\phi, h$. Rows one to three are for modes one, two and three. This is for the following parameters: $\Omega = 2.6 \times 10^{-6} s^{-1}$, $B_0 = 90T$ (these are Sun-like parameters with the exception of the background magnetic field which is stronger). The x-axis is the co-latitude and the solutions are normalized so that u_θ has a maximum of one.

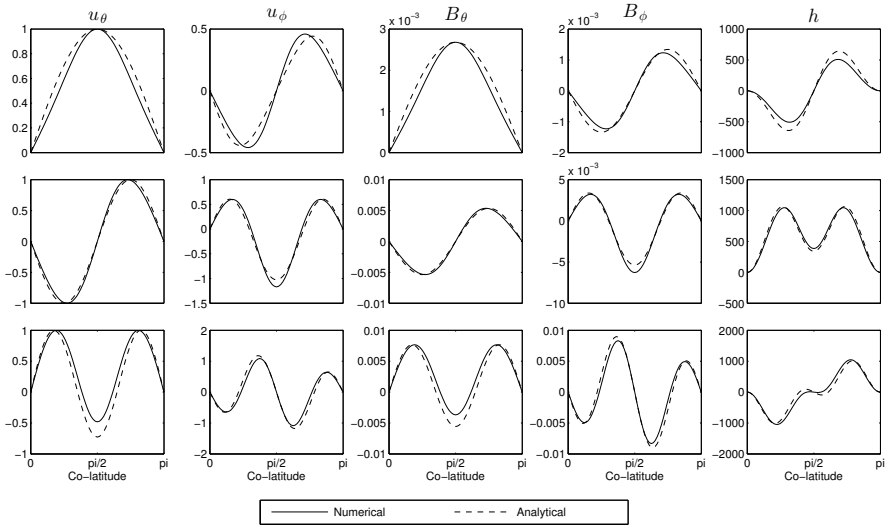

Figure 2: Comparison of the MSW modes computed numerically to the asymptotic solution presented in ZOBS [13]. Columns one to five depict the following fields: $u_\theta, u_\phi, B_\theta, B_\phi, h$. Rows one to three are for modes one, two and three. This is for the following parameters: $\Omega = 2.3 \times 10^{-5} s^{-1}$, $B_0 = 10T$ (these are Sun-like parameters with the exception of the rotation which is stronger). The x-axis is the co-latitude and the solutions are normalized so that u_θ has a maximum of one.

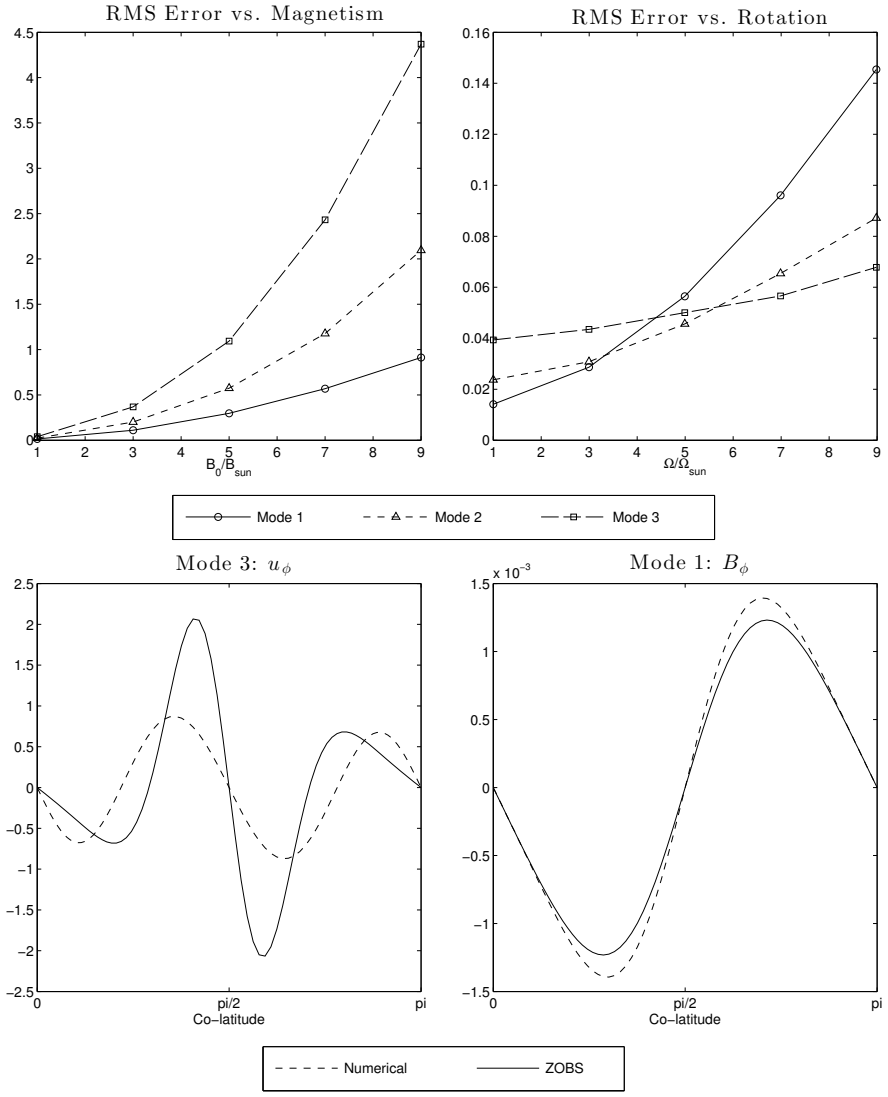

Figure 3: The top two figures illustrate how the relative root mean square (RMS) error between the numerical solution to equations (11) to (15) and equations (5) to (8) in ZOBS for the first three modes that depend on the magnetic field strength and rotation. In the top left the abscissa is the magnetic field, B_0, whereas in the top right the abscissa is the ambient rotation, Ω. The parameters are the same as used in the previous figures except for the parameter being varied. The bottom left figure compares the u_ϕ field for mode 3 in the case of the strongest magnetic field. The bottom right compares the B_ϕ field for mode 1 in the case of the strongest rotation. In both subfigures the dashed line refers to the numerical solution to equations (11) to (15), while the solid line is the solution to equations (5) to (8) in ZOBS.

what might be present in the tachocline of different stars. In the case of weak rotation and weak magnetic fields, the fields are harmonic and the analytical solution of ZOBS is accurate in describing the leading order behavior. In the Spherical formulation, when either the rotation, the magnetic field, or both become strong the error in the analytical solution increases. Similar discrepancies are observed in the Cartesian model for channel widths on the order of $\pi/10$ and only for strong rotation. Since it is well known that the Cartesian model is limited in its scope, here we focus on the modal structures in the Spherical model. We note that the qualitative dependency on the parameters in the two models are similar.

In Figure 1 we compare the five different fields, $u_\theta, u_\phi, B_\theta, B_\phi, h$, that are observed for the first three low-frequency, rotationally modified Alfvén modes that fit in the given domain in the case of strong magnetic fields in the basic state. First, we readily observe that even in this case the analytical solution agrees well with the numerical one. Indeed, the mode one structure has only slight deviations. Second, we find that the discrepancies between the mode two and three are also weak but the differences are largest in the meridional velocity, u_θ, meridonal magnetic field, b_θ and the depth, h.

The case of a rapidly rotating star is depicted in Figure 2. There are some differences that are observed but again, they are weak, and it is the meridional velocity and magnetic fields that differ the most significantly. In the case of small magnetic field and small rotation there are almost no deviations (the relative error is only one percent). We note that the discrepancies arise from the assumption of incompressibility in the analytical solution in the ϕ magnetic equation, which then impacts the ϕ velocity and height fields. This becomes apparent for higher magnetic fields because it is the evolution equation for b_θ that differs to the MSW equations given in ZOBS. Differences due to variations in the rotation are purely due to the nature of the slowly rotating star approximation used in ZOBS.

Finally, it is of interest to compare the differences between the model presented here, described in equations (11) to (15), to that in ZOBS, where the equation for the zonal magnetic field is only approximately true. This is to emphasize the error that can arise due to inaccuracies in the zonal magnetic field, given in equation (14). To do that we compare the results of applying our pseudo-spectral method to the two models and find how the relative root-mean-square (RMS) error depends on the magnetic field and ambient rotation. By relative RMS error we mean the L^2 norm of the error of the two solutions normalized by the L^2 norm of the more accurate solution. This is presented in Figure 3 for the first three modes. In the top left the abscissa is B_0 whereas in the top right it is replaced by Ω, both have the same units. The bottom left figure compares the u_ϕ field for mode 3 in the case of the strongest magnetic field. The bottom right compares the B_ϕ field for mode 1 in the case of the strongest rotation. These fields were chosen because they have the greatest relative error. The error in the case of strong magnetism is on the order of 400%, whereas the error due

to strong rotation only reaches values slightly larger than 10%. We see, perhaps not too surprisingly, that since the discrepancy is in the magnetic field, the error is more prominent with large magnetic fields. Furthermore, with varying rotation we see that the mode with the largest error depends on the magnitude of the ambient rotation whereas the error due to the magnetic field always increases with mode number (for the three modes presented). This suggests that the approximate model might be adequate for stars with relatively weak magnetic fields, as is the case for our sun, but will necessarily develop significant error for stronger magnetic fields.

4 Conclusions

We have extended the work of ZOBS and have presented a simple numerical method that can be used to compute the spectrum and spatial structures of linear MHD SW waves that can idealize those that are believed to exist in the tachocline. This is both for the Cartesian and spherical geometries. We found that even though the analytical solution in ZOBS assumes incompressibility in two spatial dimensions, it is a good approximation to the linear waves in tachoclines for stars that do not have strong magnetic fields or strong rotations. We advocate for the numerical, rather than the approximate analytical approach, because the former can determine the structure of the linear waves for a range of parameters easily.

One important point to appreciate is that with little numerical effort we can obtain accurate representation of both the spatial structures and diseprsion relations of the linear waves. This is important since the more accurately we can model waves the better we can assertain the effect they have on the transport of momentum and energy in the system. For example in the case when waves are trapped to the centre, it will be found that the transportation of momentum is more concentrated at the equator when compared to that of harmonic waves.

This study of linear waves in a solar tachocline can be extended into a nonlinear regime to determine whether the linear characteristics are maintained or, if not, what manner of changes occur. Given the nonlinear extension, it would then be possible to address the nonlinear interaction of these waves to observe what resonance mechanisms dominate in the transfer of energy between length scales. This is beyond the scope of this manuscript.

5 Appendix A

We note that equation (14) is different from equation (26) in ZOBS, which is

$$\frac{\partial b_\phi}{\partial t} = -\frac{B_0 \sin\theta}{R_0}\frac{\partial u_\theta}{\partial \theta} - \frac{B_0 \cos\theta}{R_0} u_\theta \tag{17}$$

The derivation of equation (14) involves finding the ϕ component of equation (1). In order to do so requires the identity

$$\left((\mathbf{A}\cdot\nabla)\,\mathbf{B}\right)_\phi = A_r\frac{\partial B_\phi}{\partial r}+\frac{A_\theta}{r}\frac{\partial B_\phi}{\partial\theta}+\frac{A_\phi}{r\sin\theta}\frac{\partial B_\phi}{\partial\phi}+\frac{A_\phi B_r}{r}+\frac{A_\phi B_\theta\cot\theta}{r}. \quad (18)$$

Plugging equation (18) into (1) with

$$\mathbf{B}=\begin{bmatrix}0\\ b_\theta\\ B_\phi+b_\phi\end{bmatrix},\qquad \mathbf{U}=\begin{bmatrix}0\\ u_\theta\\ u_\phi\end{bmatrix}, \quad (19)$$

we get

$$\frac{\partial b_\phi}{\partial t}+\frac{u_\theta}{r}\frac{\partial B_\phi}{\partial\theta}=\frac{B_\phi}{R_0\sin\theta}\frac{\partial u_\phi}{\partial\phi}+\frac{u_\theta B_\phi\cot\theta}{R_0} \quad (20)$$

Since $B_\phi = B_0\sin\theta$ we have $\frac{\partial B_\phi}{\partial\theta} = B_0\cos\theta = B_\phi\cot\theta$ which means

$$\frac{\partial b_\phi}{\partial t}=\frac{B_\phi}{R_0\sin\theta}\frac{\partial u_\phi}{\partial\phi} \quad (21)$$

Which is precisely our equation (14).

6 Appendix B

Since our model equations remove an extra approximation that was mode in ZOBS we now present a brief outline of the derivation of their simplified equations to see how the more general equations can be written. Multiplying equations (11) - (14) by $\sin\theta$ and (15) by $\sin^2\theta$, then substituting in $\hat{u}_\theta = u_\theta\sin\theta$, $\hat{u}_\phi = u_\phi\sin\theta$, $\hat{b}_\theta = b_\theta\sin\theta$, $\hat{b}_\phi = b_\phi\sin\theta$, get

$$\begin{aligned}
\frac{\partial\hat{u}_\theta}{\partial t}-2\Omega\cos\theta\hat{u}_\phi+\frac{g}{R}\sin\theta\frac{\partial h}{\partial\theta}-\frac{B_0}{4\pi\mu_0\rho R_0}\frac{\partial\hat{b}_\theta}{\partial\phi}+\frac{2B_0\cos\theta}{4\pi\mu_0\rho R_0}\hat{b}_\phi &= 0,\\
\frac{\partial\hat{u}_\phi}{\partial t}+2\Omega\cos\theta\hat{u}_\theta+\frac{g}{R_0}\frac{\partial h}{\partial\phi}-\frac{B_0}{4\pi\mu_0\rho R_0}\frac{\partial\hat{b}_\phi}{\partial\phi}-\frac{2B_0\cos\theta}{4\pi\mu_0\rho R_0}\hat{b}_\theta &= 0,\\
\frac{\partial\hat{b}_\theta}{\partial t}-\frac{B_0}{R_0}\frac{\partial\hat{u}_\theta}{\partial\phi} &= 0,\\
\frac{\partial\hat{b}_\phi}{\partial t}-\frac{B_0}{R_0}\frac{\partial\hat{u}_\phi}{\partial\phi} &= 0,\\
\sin^2\theta\frac{\partial h}{\partial t}+\frac{H_0}{R_0}\left(\sin\theta\frac{\partial\hat{u}_\theta}{\partial\theta}+\frac{\partial\hat{u}_\phi}{\partial\phi}\right) &= 0.
\end{aligned}$$

If one follows steps similar to those in ZOBS one can reduce this system to one equation for the dispersion relation. This requires defining the following

parameters

$$\lambda = \frac{\omega}{2\Omega}, \quad \varepsilon = \frac{4\Omega^2 R_0^2}{gH_0}, \quad \alpha^2 = \frac{B_0^2}{16\pi\mu_0\rho\Omega^2 R_0^2}, \tag{22}$$

$$\eta = \frac{gh}{2\Omega R_0}, \quad \mu = \cos\theta, \quad D = (1-\mu^2)\frac{\partial}{\partial\mu}, \tag{23}$$

and one obtains that the full dispersion relation is

$$\Big[\Big[\left(\lambda\mu + 2s\mu\alpha^2\right) s\lambda + \left(\lambda^2 - s^2\alpha^2\right)\lambda D\Big] \times \frac{\left(\lambda^2 - s^2\alpha^2\right) D - s\left(\lambda\mu + 2s\mu\alpha^2\right)}{\varepsilon\lambda\left(1-\mu^2\right)\left(\lambda^2 - s^2\alpha^2\right) - s^2\lambda} - \left(\lambda\mu + 2s\mu\alpha^2\right)^2 + \left(\lambda^2 - s^2\alpha^2\right)^2\Big]\tilde{u}_\theta = 0 \quad .$$

If one makes the approximations that $\frac{\varepsilon}{s^2} \ll 1$ and $\alpha^2 \ll 1$, essentially that the rotation and magnetic fields are relatively small, then we can approximate the equation with the Legendre differential equation:

$$\left[\frac{\partial}{\partial\mu}\left(1-\mu^2\right)\frac{\partial}{\partial\mu} - \frac{s^2}{1-\mu^2} + \frac{s}{\lambda}\right]\tilde{u}_\theta = 0.$$

Now note that we have defined $D\mu = \left(1-\mu^2\right)\frac{\partial}{\partial\mu}\mu = \left(1-\mu^2\right) + \mu\left(1-\mu^2\right)\frac{\partial}{\partial\mu} = (1-\mu^2) + \mu D$. This is precisely the Legendre equation with $n(n+1) = -\frac{s}{\lambda}$ and the solutions are of the form $\tilde{u}_\theta = P_n^s(\cos\theta)$. This is the solution found in [5].

7 Acknowledgements

F.J.P and M.S. would like to thank the Natural Sciences and Engineering Research Council of Canada and B.A.S would like to thank the Ontario Graduate Scholarship for financial support during this research.

References

[1] Bouchut, F., and Lhbrard, X. (2016). A 5-wave relaxation solver for the shallow water MHD system. Journal of Scientific Computing, 68(1), 92-115.

[2] Charbonneau, P., Christensen-Dalsgaard, J., Henning, R., R.M., L., Schou, J., Thompson, M., Tomczyk, S., 1999. Helioseismic constraints on the structure of the solar tachocline. Astrophys. J. 527, 445–460.

[3] Gilman, P., 2000. Magnetohydrodynamic "shallow water" equations for the solar tachocline. ApJL, 544.

[4] Heng, K., Spitkovsky, A., 2009. Magnetohydrodynamic shallow water waves: linear analysis. Astrophys. J. 703 (2), 1819–1831.

[5] Longuet-Higgins, M., 1965. Planetary waves on a rotating sphere. II. Proc. Roy. Soc. A. 284, 40–54.

[6] Miesch, M., 2005. Living rev. sol. phys.,. [Online Article], http://www.livingreviews.org/lrsp–2005–1.

[7] Pedlosky, J., 1987. Geophysical Fluid Dynamics. Springer-Verlag.

[8] Poulin, F., Flierl, G., 2003. The nonlinear evolution of barotropically unstable jets. J. Phys. Oceangr. 33 (10).

[9] Raphaldini, B., and Raupp, C.F.M., "Nonlinear Dynamics of Magnetohydrodynamic Rossby Waves and the Cyclic Nature of Solar Magnetic Activity." The Astrophysical Journal 799.1 (2015): 78.

[10] Schecter, D., Boyde, J., Gilman, P., 2001. "shallow-water" magnetohydrodynamic waves in the solar tachcline. Astrophys. J. 551, 185–188.

[11] Spiegel, E. A., Zahn, J.-P., 1992. The solar tachocline. Astronomy and Astrophysics 265 (1), 106–11.

[12] Trefethen, L., 2000. Spectral Methods in MATLAB. SIAM.

[13] Zaqarashvili, T. V., Oliver, R., Ballester, J. L., Shergelashvili, B., 2007. Rossby waves in "shallow water" magnetohydrodynamics, A&A, 470, 815–820.

[14] Zaqarashvili, T. V., Oliver, R., Hanslmeier, A., Carbonell, M., Ballester, J. L., Gachechiladze, T., and Usoskin, I. G. (2015). Long-term variation in the Suns activity caused by magnetic Rossby waves in the tachocline. The Astrophysical Journal Letters, 805(2), L14.

Received January 2017; revised December 2017.

email: journal@monotone.uwaterloo.ca
http://monotone.uwaterloo.ca/∼journal/